Journal of Hard Tissue Biology 23[4] (2014) 423-434

CODEN-JHTBFF, ISSN 1341-7649

Original

The Ceramics Radiating Far Infrared Ray Energy (Rhyolite) Promote the Formation of Bone

Aldartsogt Dolgorsuren[1, 2], Kikuji Yamashita[1], Shine-Od Dalkhsuren[2], Kaori Sumida[1], Shinichiro Seki[1] and Seiichiro Kitamura[1]

[1] Department of Oral and Maxillofacial Anatomy, Graduate School of Oral Sciences, the University of Tokushima, Tokushima, Japan
[2] Departments of Gross Anatomy, School of Bio-Medicine, Health Sciences University of Mongolia, Ulaanbaatar, Mongolia
(Accepted for publication, September 1, 2014)

Abstract: Far infrared ray (FIR) energy radiated by the natural ceramics (Rhyolite) cooled FIR ceramics activates water molecules and blood circulation to stimulate skin and other tissues. The aim of our study is to make clear whether the FIR ceramics radiating FIR energy affect or not on the new bone formation *in vivo* and *in vitro*. Methods: MC3T3-E1 cells were cultured in FIR CO_2 incubator. The cell proliferation and the gene expression were analyzed by using WST-8 assay kit, RT-PCR and micro array analysis. The enzyme activities were analyzed by using the api^{R}ZYM kit. Furthermore, titanium and natural FIR ceramics compounds were implanted under the periosteium of rat skull bone by injection method. Four weeks later, the samples were examined by the light microscope and micro CT analyses. Results: Proliferation of MC3T3-E1 cell was and DNA concentrations were inhibited by FIR energy radiation. The ALP activities were accelerated and the area of calcification nodules increased on 4 weeks. The RT-PCR data showed that the gene *Runx2, Osterix, BSP*, *OCN, Col1a1 and OPN* expression of MC3T3-E1 osteoblast like cells was activated. Bone mineral density (BMD mg/cm²) of implanted sites of T50-F50, T25-F75 and F100 groups was significantly enhanced after 4 weeks compared with control groups. This data shows FIR energy radiation by the natural FIR ceramics promoted bone-forming activity of osteoblasts. Significance: This study suggested that new bioactive ceramics such us natural FIR ceramics was useful for some clinically applications to repair bone defects for example of dental implant surgery.

Key words: Bone formation, Far-infrared ray, Osteoblast

Introduction

Bone is a mineralized connective tissue continuing to be remodeled throughout lifetime. It has also the important multifunction's including mechanical protection for organs, hematopoiesis and mineral storage[1-4]. The bone is some time injured by high force impact trauma, as surgical removing of tumors, age related disorders and loss of structural integrity of the bone[5,6]. However the perfect healing for fracture nonunion and tumor recovering becomes difficult, when an area of damaged bone is too large to be self-repaired. Then, the intense damaged bone must be repaired by using any alternative material such as autografts, allografts, and artificial materials. Therefore, autografts and allografts considered best selection, but these supplies are limited. Synthetic bone graft substitutes as next available can provide a scaffold for bone to repair[7]. Recently, many synthetic bone grafting materials including polymers[8], hydroxyapatite[9,10], calcium phosphate[11], metals[12,13], bioactive glasses[14-16] and glass ceramics[17,18] have been used for repair and restoration of bone defects, but their osteoinductive properties were not sufficient to induce new bone formation.

Besides angiogenesis may also play a crucial role in the remodeling and healing process. Bitto A and Minutoli L et al reported that angiogenesis and neovascularization can help and alleviate these certain diseases[19]. This process associated with the expression of cytokines, as well as angiogenic factors such as VEGF. Moreover, that the smooth vascular muscles expand is to deliver oxygen for connective tissue and also increased blood flow velocity[20]. It was well known that FIR energy radiation can heat and activate blood circulation of living bodies[21,22].

Then, we evaluate comparatively various materials with FIR energy radiation power and selected bioactive natural FIR ceramics. The natural FIR ceramics was the excellent radiator which radiation rate was almost 90 % of FIR energy of 5~20 μm and good scaffold for cell migration[23-25]. It was suggested in our previous study that the rhyolite radiating FIR energy activated

Correspondence to: Dr. Kikuji Yamashita, Department of Oral and Maxillofacial Anatomy, Institute of Health Bioscience, the University of Tokushima, 3-18-15 Kuramoto, Tokushima, 770-8504 Japan; Tel: +81-88-633-9120; Fax: +81-88-633-7320; E-mail: yamashita.kikuji@tokushima-u.ac.jp

water molecules and blood circulation to stimulate skin and other tissue[26-28]. Moreover, FIR energy helps to increase the metabolism by expanding blood capillaries stimulating blood circulation and increasing oxygenated metabolism of peripheral tissue to promote tissue regeneration[29]. However, the details are still poorly understood. Several studies showed that FIR therapy has been applied to various clinical fields, including vessel related disorders. Huang PH and Chen JW et al reported that the administration of FIR therapy significantly improved collateral blood flow recovery and new vessel formation[30]. Recently, Inoue S and Takemoto M et al demonstrated that Leg thermal therapy of heating was far infra-red increased the antioxidative stress marker as Thiol, and the antioxidant enzyme as GPx, and serum VEGF[31]. It was also the marker of oxidative DNA damage as urine 8OHdG significantly decreased after the leg thermal therapy. Still more, it also detected and improves the activity of vagal nerves, the endothelial function and hemodynamic factors. Therefore, FIR in our investigation was to be evaluating the importance for bone induction. But it was not clear that the natural FIR ceramics with FIR radiation was useful or not for bone formation. In order to make clear how the natural FIR ceramics radiating FIR affect new bone formation, the experiment in vitro and *in vivo* was carried out.

Materials and Methods

FIR incubator

As previously reported, the incubator has a stably irradiate system with FIR at wavelengths between 4 and 20 μm under conditions of 90-100 % humidity, 37±0.5 °C and 0.5% CO_2 in air (Fig.1A).

Alpha modified Eagle's Minimum Essential Medium (α-MEM) was purchased from Invitrogen (Gibco, Grand Island, NY, USA). Plastic dishes were from TPP (Techno Plastic Products AG, Zollstrasse, Switzerland) and fetal bovine serum (FBS) was from Biosera (Dominican Republic Origin). L-ascorbic acid and β-glycerophosphate were purchased from Sigma-Aldrich Chemie (Gmbh, Steinheim, Germany).

Cell culture and osteogenic induction

Cells were cultured in α-MEM supplemented with 10% FBS, 100μg/ml penicillin, 100 μg/ml streptomycin sulfate in humidified atmosphere 5 % CO_2 at 37 °C. When cells reached 90 % confluence on two or three days after plating 6 well plates, they were subsequently cultured for 3, 7, 14 and 21 day in induction of osteoblast differentiation medium supplemented with 50 μm ascorbic acid, and 10 mM β-glycerophosphate. Then, cell cultures were separated to two groups of FIR radiating group and control group. The FIR group was maintained in FIR energy radiating incubator for one hour every day. The medium of the cultured cells was changed every 3 days.

Proliferation assay

Approximately 10^4 MC3T3-E1 cells were placed in each well of a 96 well microplate TPP (Techno Plastic Products AG, Zollstrasse, Switzerland). Cell proliferation was estimated by using WST-8 assay kit on 0, 3, 7, 14 and 21 days. The medium was absorbed and the cells each well were added with the 100 μl medium and 10 μl of the WST-8 assay solution. The plate was incubated at 37 °C for 4 hours and proliferating cells in each well were estimated by measuring with the microplate reader (ImmunoMini NJ-2300, System Instruments Co., Tokyo, Japan) at 450 nm.

Determination of alkaline phosphatase (ALP) activity

The measurement of ALP activity was performed on 0, 3, 7, 14 and 21 days. Cultured osteoblast cells in differentiation medium was removed and rinsed with phosphate-buffered saline (PBS) by three times. Cells were lysed by 50 mM Tris-HCI buffer (pH7.4), sonicated for 15 seconds using the Branson Ultrasonics (Sonifier 250, Eagle Rd., Danbury, NY, USA) and centrifuged at 10.000 rpm for 15 min at 4 °C. Twenty microliters of cell lysate was mixed with 100 μl of p-Nitrophenylphosphate (Wako Pure Chemical Industries Co. Ltd., Osaka, Japan), then incubated at 37 °C for 30 minutes after the reaction was stop by adding 80 μl of 0.2 mol/l sodium hydroxide solution, the solution was measured in a microplate reader at 405 nm.

ALP and alizarin red histochemical staining

Cultured on 3, 7 14 and 21 days cells in osteoblast differentiation, the cells were rinsed with Ca–Mg free phosphate–buffered saline by three times. The cell were fixed with 3.5 % methanol paraformaldehyde for 2 min at -3 °C do -5 °C according to the manufacture's protocol of ALP and Acid Phosphatase (AP) Kit. For Alizarin red staining, cells cultured for 2, 3, and 4 weeks rinsed with PBS twice, fixed 3.5 % methanol formaldehyde for 10 min, and then stained with 2% Alizarin red (Wako Pure Chemical Industries Co. Ltd., Osaka, Japan) at pH 4.2 for 15 min.

RNA isolation and real-time polymerase chain reaction analysis

Total RNA was extracted from MC3T3-E1 cultured cells by using Trizol reagent (Invitrogen, Tokyo, Japan). The cells were homogenized in 1 ml of Trizol reagent and isolated RNA was used for reverse transcription reaction with Prime Script reverse transcription kit (Toyobo Co. Ltd., Osaka, Japan) to obtain cDNA. Real-time PCR of each gene was performed with a 7300 Real-time PCR system (Applied Bio-systems, Carlsbad, CA, USA) using SYBER Premix Ex Taq™ (Takara Bio Inc., Otsu, Japan) in triplicate for at least three independent experiments. The sequence of the primers was as follows: Mouse Gapdh forward, 5'-CAAAGTTGTCATGGATGACC-3', reverse, 5'-CCATGGAGAAGGCTGGGG-3', mouse Runx2 forward, 5'-

TGCTCTGTTCCAAGCGCTTT-3', reverse, 5'-TGGGTGCGCTGATGTTTG-3', mouse BSP forward, 5'-CCAAGAAGGCTGGAGATGCA-3', reverse, 5'-TCCTCGTCGCTTTCCTTCAC-3', mouse Osterix forward, 5'-CCTGCCTGCTCTGTTCCAA-3', reverse, 5'-GGGTGCGCTGATGTTTGC-3', mouse OCN forward, 5'-CTGACAAAGCCTTCATGTCCAA-3', reverse, 5'-AGGTAGCGCCGGAGTCTGTT-3', mouse OPN forward, 5'-TCCCGGTGAAAGTGACTGATTC-3', reverse, 5'-TGGGTGCAGGCTGTAAAGCT-3' and mouse Collagen type 1a1 forward, 5'-GCGATGACGTGCAATGCA-3', reverse, 5'-CACTCGCCCTCCCGTCTT-3'.

Microarray analysis

The total RNA of the MC3T3-E1 cultured cells in control and FIR incubator on 3 and 7 day (each group n = 4) was extracted using RNeasy plus Mini kit (Qiagen, Geschäftsführer, Germany). After ascertaining that A260/A280 ratio was over 1.9 using the UV spectrophotometer (Nano Drop 1000, Thermo Fisher Scientific, Wilmington, DE, USA), no RNA degradation was assured by using Agilent 2100 Bioanalyser (Agilent Technologies, Palo Alto, CA, USA). RNA amplification was then labeled with the Low RNA Input Fluorescent Linear Amplification Kit (Agilent Technologies, Santa Clara, CA, USA). The hybridization was performed according to the protocol of the Whole Rat Genome Oligo DNA microarray kit Ver.3.0 which loads around 27,000 representative rat genes. The fluorescence of Cy3 and Cy5 were scanned at 670 nm and 770 nm, respectively, using the DNA Microarray scanner. The significant expressions of the extracted genes were analyzed by using Gene Spring 7.0 software (Silicon Genetics, Santa Clara, CA, USA). The intensity-dependent LOWESS per spot and per chip normalization was demonstrated.

Enzyme activity/api ^{R}ZYM test/

The MC3T3-E1 cultured cells were diffused in 500 µg/ml in PBS of 1 ml and homogenated using the sonicator (Sonifier 250, Eagle Rd., Danbury, NY, USA).The metabolic enzyme activity of prepared samples were measured by means of the api^{R}ZYM test (bioM'erieux, Marcy l'Etoile, France) according to manufactures protocol.

Animal experiment

Ten male Sprague Dawley rats (SD, male, 4 weeks, SPF/VAF) of four week old were purchased from Charles River (Yokohama, Japan). The rats were randomly divided two groups CTR and FIR radiation treatment group. In additionally animal raising FIR incubator was utilized. The animal were housed in an experimental animal room (22 °C, 55 % relative humidity and a 12 h light/dark cycle) and fed a standard laboratory diet. The experimental protocol described below was approved by the Ethical committee of the University of Tokushima (Permit number 11110).

Animal raising FIR incubator

The FIR animal raising apparatus with same FIR radiating system of the FIR CO_2 incubator to control the inside temperature 20-40 °C reduces various smell chemical products by photo-degradation with the light catalyst of TiO_2. The FIR animal raising apparatus has the two chambers which the upper chamber is coated with the valid FIR ceramics containing and the lower chamber is no coating. A carbon /silica/aluminum oxide/titanium oxide ceramics (radiating efficiency > 97 %). The incubator can stably irradiate FIR at wavelengths between 4 and 20 µm (maximum at 7 to12 µm) under the condition of 90-100% humidity, 37±0.5 °C and 5 % CO_2 in air.

Implanted materials

Natural FIR ceramics and titanium was purchased from (MATERA Inc., Toon, Japan), (RTP post titanium # Ti, Dentech, Tokyo, Japan). We were prepared five kind compounds. FIR ceramics 100 %, FIR ceramics 75 % with Titanium 25 %, FIR ceramics 50 % with Titanium 50 %, FIR ceramics 25 % with Titanium 75 % and 100 % pure Titanium. Briefly, 50 mg total composite suspension was suspended in to 300 µl of the same amount of cell matrix (Cell matrix Type1-A, Nitta gelatin Co. Ltd., Osaka, Japan) and PBS (natural FIR ceramics specific gravity 2.43, grain diameter of 10 µm, titanium specific gravity 4.5 and grain diameter of 45 µm) was incubated under sterile conditions. 100 µl compounds were implanted under the periosteium of rat calvaria bone by the injection method under the anesthesia.

Microcomputed tomography image (µCT)

Dissected rat calvaria with implanted compound were fixed and analyzed by micro CT system (Latheta^{TM} LTC-200, Hitachi Aloka Medical Ltd., Tokyo, Japan). Bone mineral density (BMD) mg/cm^3 was calculated by micro CT analysis.

Histological analysis of bone tissue sample

The parietal bone of rat calvaria at 9 weeks after the operation was fixed in 4% formaldehyde (PFA) in PBS for 4 hours at 4 °C, and embedded in paraffin by usual method. The embedded samples were consecutively cut into 7 µm thick sections with microtome (Microm, Walldorf, Germany) and stained with Heamatoxylin and Eosin (H&E). The stained sections were observed with the light microscope (BX51, Olympus Optical Co. Ltd., Tokyo, Japan).

Statistical analysis

Each *in vitro* experiment was repeated three times. In the case of cell proliferation, ALP activity, enzyme activity AP, nodule formation and real-time PCR, the results obtained from a typical

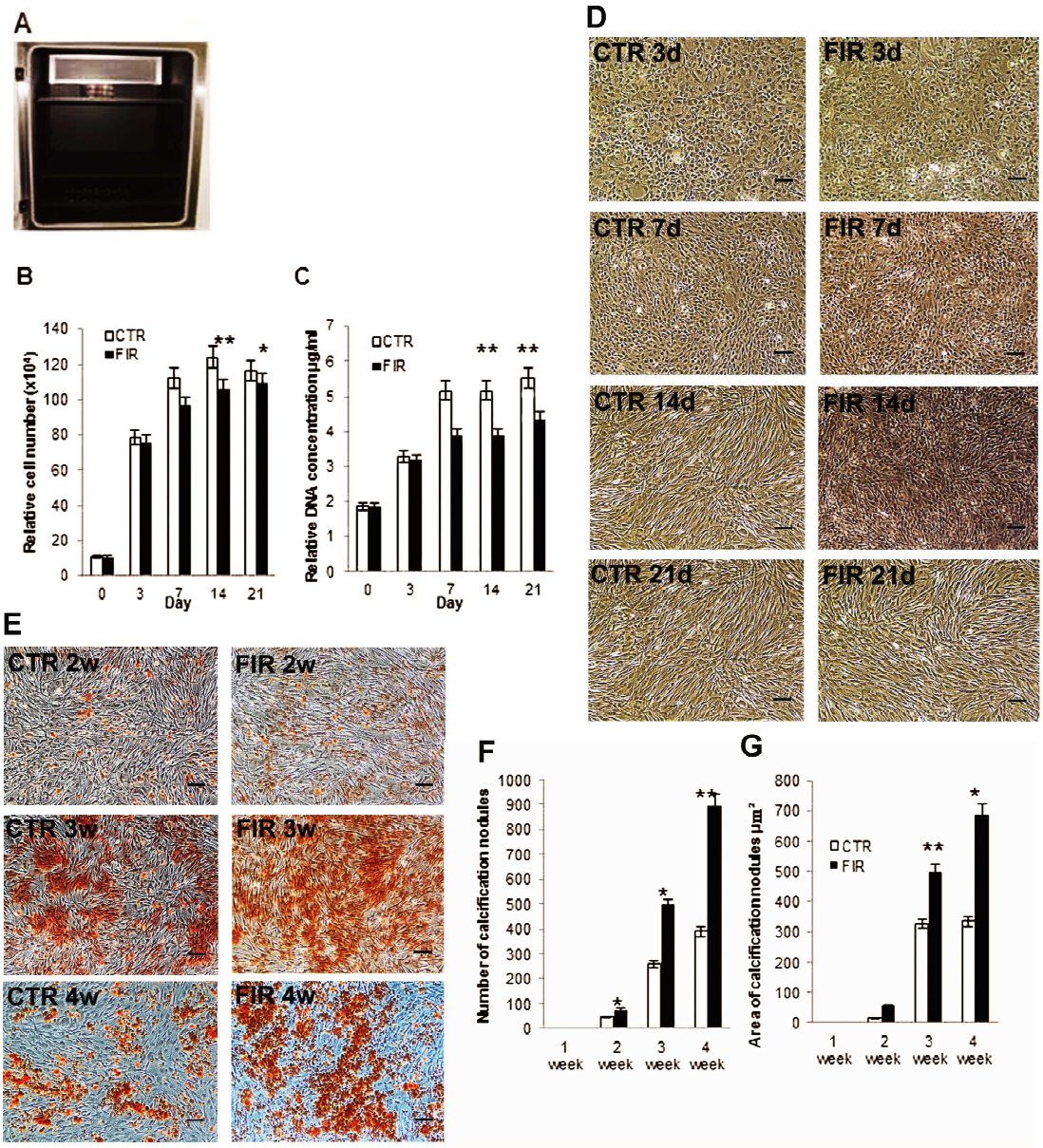

Figure 1. The effects of FIR on cell growth and mineralization of cultured MC3T3-E1 cells. The FIR CO_2 Incubator for cell cultures (A). The proliferation of MC3T3-E1 cells were inhibited on day 14 and 21 respectively (B), DNA concentrations in the cultured cells were decreased on day 14 and 21 (C), Data presented are from two independent experiments, with triplicate samples per each experiment. A representative morphological image of MC3T3-E1 cultured cells was observed by inverted stage microscope (D). Pictured, were shown in Fig E, F, G the formation of the mineralized nodules in the FIR group was more than the control group by the observation of the cultured cells stained with Alizarin red (E). The bone nodules number and area was gradually increased (F and G). Each bar represents the mean ± S.E. * $p<0.05$, ** $p<0.01$. (G). Scale bars indicate 100 μm.

experiment in three separate experiments (triplicate cultures) were expressed as the means ± SD (n = 3). The significance of differences between two groups was calculated with the unpaired Student's *t* test. The results are expressed as the mean ± SD for each group. Values of $p<0.05$ and $p<0.01$ were considered statistically significant.

Results

Proliferation and bone formation

To evaluate the effects of FIR on MC3T3-E1 cell proliferation, the cell numbers and DNA concentrations were assays. The number of MC3T3-E1 cells in FIR treated group was decreased by 13.8 % at 7 day and 14.7 % at 14 day in Fig. 1B. Similar result was obtained by BCA protein assayed. Synthesis of DNA by incorporated BCA of FIR treated group was also inhibited by 25.1 % at 7 day and 25.4 % at 14 day respectively as compared with control (Fig. 1C). Triplicated measurements were done on each experiment. Figure 1D shows viable cell were photographed by

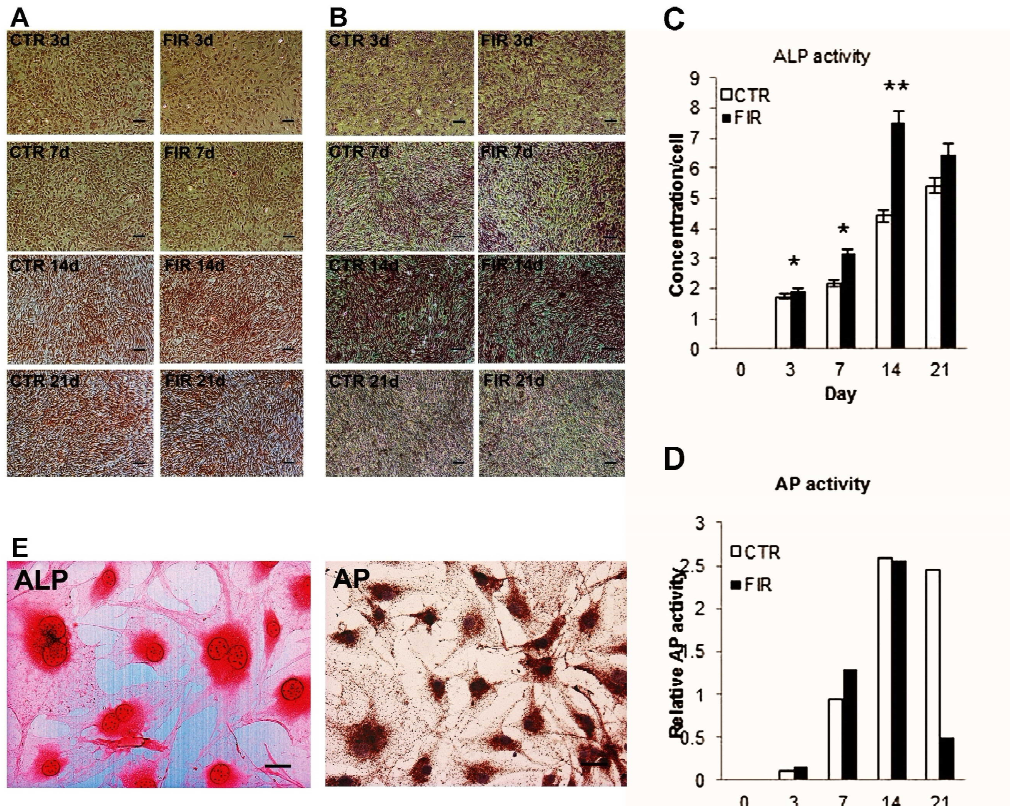

Figure 2. Effects of FIR energy on alkaline phosphatase and acid phosphatase activity in MC3T3-E1 cells. In order to estimate the effect of FIR in osteoblast differentiation, ALP and AP were stained (A, B) and quantitate the activities. The ALP activity increased in time of control and FIR group up to 14 days. The level of ALP in FIR group was activated on 3, 7 and 14 days and it was slightly decreased on 21 days (C). The acid phosphatase activity increased also in time of control and FIR group up to 14 days. The activity of AP in FIR group was activated on 7 day also. Then the activity of AP in 14 day was same and that 21 day decreased as compared control group (D). The localization of ALP and AP in osteoblast like cells compared at 3 day after culture. The (ALP) was localized near nuclei. (E). In contrast, acid phosphatase widely scattered in cytoplasm (E). Each bar represents the mean ± S.E. * $p<0.05$, ** $p<0.01$. (G). Scale bars indicate 400 μm.

inverted stage microscope (Nikon Eclipse TE300, DS-L3, Nikon Co., Tokyo, Japan), and related calculation was done (Fig. 1B and 1C). Bars indicate 100μm. Though the cell shapes changed from spindle shape on day 3 to polygonal shape on day 7, it was not able to find any morphological difference of MC3T3-E1 cells between experimental and control groups.

The results evaluated calcification of bone nodules in vitro showed by photograph and the graph of number and area of calcification nodules. The formation of the calcified nodules in the FIR group was more than the control group by the observation of the cultured cells stained with Alizarin red (Fig. 1E). Bars indicate 100 μm. FIR treatment group were 76 and 55.22 μm^2 on 2 weeks, 495 and 500.1 μm^2 on 3 weeks, 895 and 685.7 μm^2 on 4 weeks respectively as compared with control groups (Fig. 1F and 1G). Therefore the formation of calcified nodules was clearly promoted by the FIR radiation.

ALP and AP activity increased during MC3T3-E1 differentiation

To clarify further the role of FIR in osteoblast differentiation, ALP, and AP were stained in Fig. 2A, 2B and 2E and measured by quantitative analysis in Fig. 2C and 2D. The intensity of the staining of ALP and AP increased in cultured cells of the FIR treatment group as compared with that in control group cells in early stage. The level of ALP activity increased in a time dependent manner up to 14 days, and it was slightly decreased at 21 day. ALP activity of FIR treatment group was accelerated by 5.9 % at 3 day, 25 % at 7 day and 65 % at 14 day respectively as compared with control group (Fig. 2C). In contrast the AP activity increased with time and the highest activity of AP was on 14 day in FIR treatment group in Fig. 2D. It means that AP activity was affected on early stage of osteoblast like cell cycle. Both ALP and AP showed higher activity on 14 days and 7 days respectively after cell culture for each important of osteoblastic differentiation in Fig. 2D. The localization of ALP and AP in osteoblast like cells was compared at 3 day after culture (Fig. 2E). Interestingly, the localization of ALP and AP was different. It was made clear that the ALP was localized near nuclei (Fig. 2E). In contrast, AP widely scattered in cytoplasm (Fig. 2E). Localization of AP indicates that the AP expression of cytoplasm was induced during osteoblast differentiation. Bars indicate 100μm.

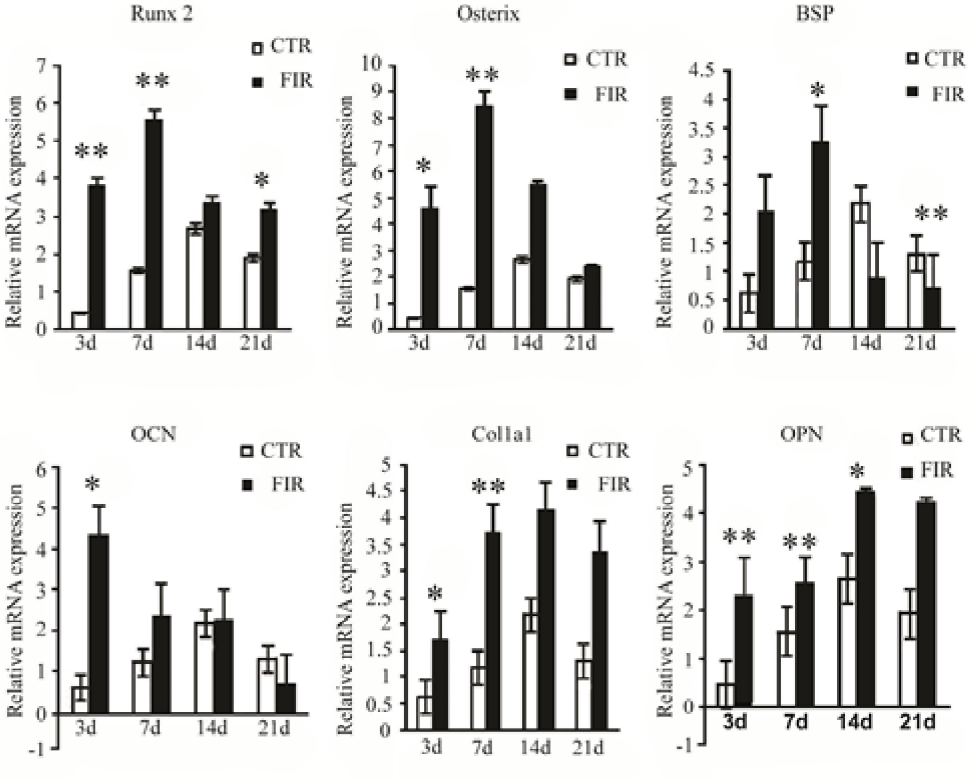

Figure 3. Effects of FIR energy on the expression of bone related genes during osteoblast differentiation. The gene expression of Runx2 significantly increased by 3.8 and 5.4 fold time and 2.9 fold times on 3, 7 and 21 days. Still more, the gene expression of Osterix increased by 4.6 and 8.6 fold-times on respectively 3 and 7 days. BSP increased only by 3.2 and fold-times on 7 day and 0.6 fold times decreased on 21day, OCN by 4.3 fold-times on 3 days increased by respectively. The gene expression of Col 1a1 increased by 1.7 fold-time on 3 day, 3.8 fold-time on 7 day and that of OPN increased by 2.3 and 2.6 fold-time on 3d, 7d, and 4.5 fold-time on 14 day by real-time PCR with normalization by GAPDH expression. Each bar represents the mean ± S.E. * $p<0.05$, ** $p<0.01$.

Gene expression

To investigate the molecular mechanism in the osteoblast differentiation by FIR treatment, the expressions of several bone related genes were examined in the control and FIR treated cells by real-time PCR. The gene expression of Runx 2 significantly increased by 3.8 and 5.4 fold time, Osterix by 4.6 and 8.6 fold-time on respectively 3 and 7 days. Still more, the gene expression of BSP only by 3.2 fold-times on 7 day, OCN by 4.3 fold-times on 3 days increased by respectively. The gene expression of Col 1a1 increased by 1.7 fold-times on 3 day, 3.8 fold-times on 7 day and that of OPN increased 2.3 and 2.6 fold-times on 3d, 7d, and 4.5 fold-times on 14 days by real-time PCR with normalization in Fig. 3.

cDNA microarray analysis was performed in order to elucidate the influence of FIR in vitro on the expression of genes. It was selected that changed genes by FIR on MC3T3-E1 cells were listed in Table 1 as over the 1.3 and Table 2 as lower the -1.3. It was also made clear that the gene expression of microarray data shown Smad 7, Tgfbi, VEGF related Chd3, Sp100, DEAD related Ddx 46, 58, Thyroid hormone related Trip13, PDGE related Pdgfd Interleukin related IL15ra, Fndc1 and Sema 4a, Sema 4g were clearly activated (Table 1). Then the gene expression of Pdgfb B polypeptides, interleukin 17b, IL17c, IL3 Thrap3 were oppositely inhibited (Table 2). It was reported that *Smad 7* bound the BMP1 receptor to inhibit differentiation of osteoblast by Smad pathway. Also it was known that genes of Ddx 46, Ddx 56, Fndc1, Trif 13, were related metabolism and binding cell binding. But our results suggested that FIR activated the differentiation of osteoblast. Therefore it was suggested that SP100 and Chd3 activated the gene expressions of Runx2 and Osterix to precede the differentiation of osteoblast by Notch pathway.

In vivo experiment

To examine the role of FIR in bone formation *in vivo*, the compounds of natural FIR ceramics and titanium with cell matrix implanted under periosteium of rat calvaria region and observed by digital photograph (Fig. 4A). In the case of (F75 % with T25 %) and pure FIR ceramics (FIR ceramics 100 %) cell migration and new vascularization were strongly activated. Then, we found the new blood vessels around implanted site and makes marks green arrow heads (Fig. 4B). Local administration of FIR group was affected of bone formation in rat calvaria as demonstrated by μCT images (Fig. 4C). Bone mineral density (BMD mg/cm^2) was

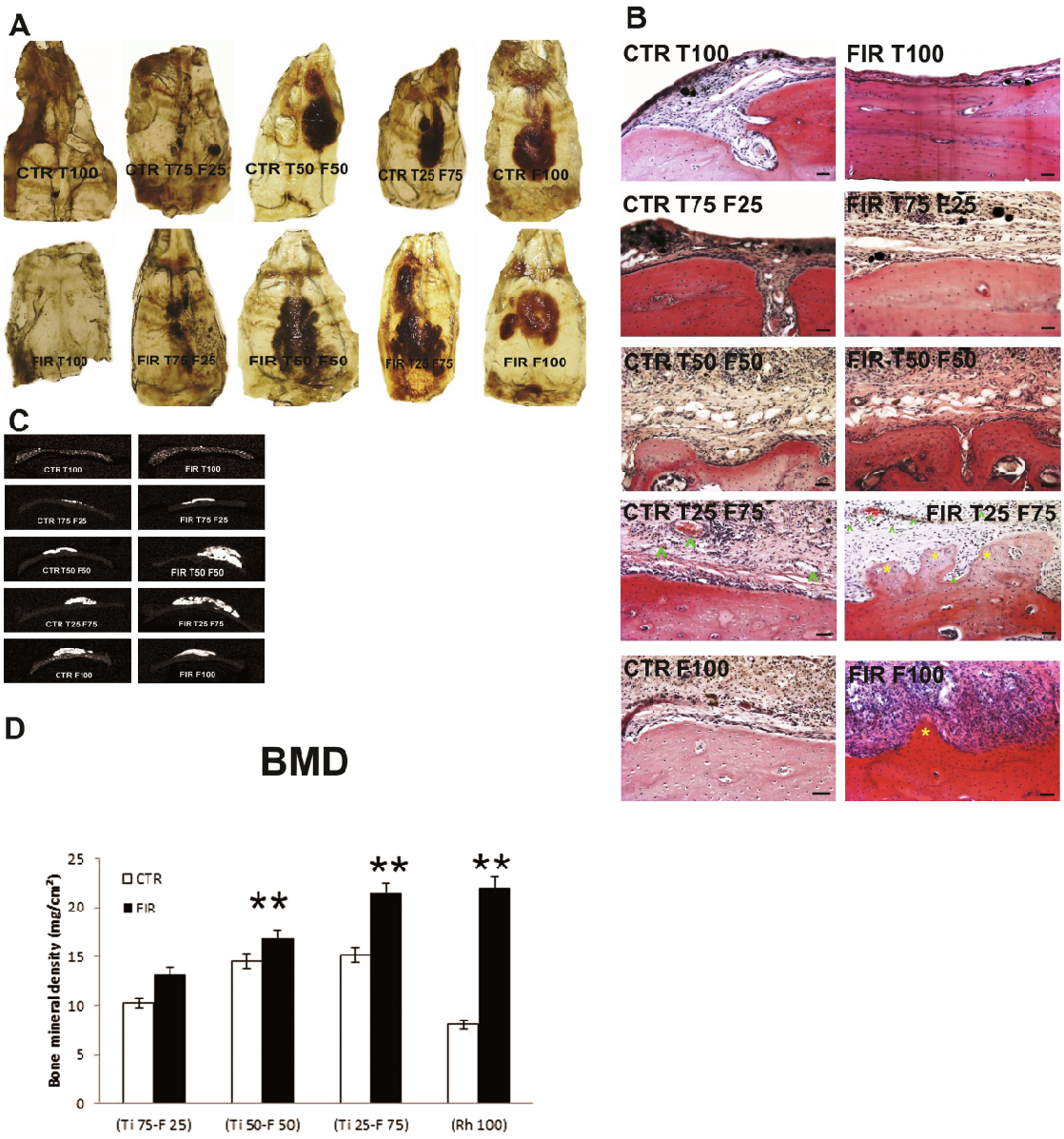

Figure 4. Effects of natural FIR ceramics radiating FIR energy on new bone formation of calvaria bone. The photographs of implanted compound representative transparent macroscope on the calvaria bone by on 4 week after operation (A). New bone formation was detected in the group of T25 F75 and pure FIR ceramics additionally FIR treatment groups (yellow asterisk) and new vascularization marks green arrow heads by H&E staining (B). Left panel is indicated the Micro focal computed tomography images of rat calvaria control groups, right panel is indicated additionally FIR treatment group. (8 weeks old) (C). Cortical bone mineral density (BMD) of calvaria bone was determined by iCT analysis (D). Bone mineral density was significantly enhanced after 4 weeks group of T50-F50 by 16.86 mg/cm^2, T25-F75 21.43 mg/cm^2 and pure FIR 22 mg/cm^2. Data are presented as means± S.E. ** p< 0.01. Scale bars indicated 100μm.

significantly enhanced after 4 weeks group of T50-F50 by 16.86 mg/cm^2, T25-F75 21.43 mg/cm^2, and pure F22 mg/cm^2 by additionally FIR treated group compared with control groups (Fig. 4D).

Discussion

It was suggested that FIR radiation activated ALP and AP activity to form the bone nodules in the present study. These results provided the evidence that FIR energy was a novel responsible factor for osteoblast differentiation in vitro. Sheppard AR et al have studied that the effect of FIR treatment induced the biological structures including cells, cell membranes; cell fluids-especially water and DNA proteins[32]. FIR energy is absorbed by vibrational levels of bonds in water molecules. Considering the high contents of water in biological systems, association of water molecules with ions, the dielectric properties of the water and the large dipole moment that this effect generates, this will be a dominant factor in biological solutions. It is known that lower frequencies water molecules are able to rotate freely in an oscillating electric field with little or almost no energy loss. In

Table 1. List of activated genes of MC3T3 cells by FIR energy

Gene name	Fold change	Acc.No	Description
Transcription			
Chd3	2.276	AK045449	Chromo domain helicase DNA binding protein 3
Ddx46	2.012	BC019403	DEAD (Asp-Glu-Asp) box polypeptide 46
Smc2l1	1.961	NM_008017	SMC2 structural maintenance of chromosomes 2-like 1
Mphosph1	1.788	AK049225	M-phase phosphoprotein 1
Smarca2	1.659	AK020092	SWI/SNF related, matrix associated, actin dependent regulator of chromatin, subfamily a, member 2
Smad7	1.685	NM_008543	Mus musculus MAD homolog 7(Drosophila) (Smad7), mRNA.
Ifi205	1.597	NM_172648	Interferon activated gene 205
Sp100	1.586	NM_013673	Nuclear antigen Sp100
Pabpc1	1.545	NM_008774	Poly A binding protein, cytoplasmic 1
Ddx58	1.531	BC027369	DEAD (Asp-Glu-Ala-Asp) box polypeptide 58
Helic1	1.528	AK052745	Activating signal co integrator 1 complex subunit 3
Dna21	1.434	BC025182	DNA2 DNA replication helicase 2-like yeast)
Cell –cell signaling			
Ifi205	1.597	NM_172648	Interferon activated gene 205
Sp100	1.586	NM_013673	Nuclear antigen Sp100
Pdgfd	1.555	AK003359	Platelet-derived growth factor, D polypeptide
Sema4a	1.454	NM_013658	Semaphoring 4A
Cdc27	1.432	BC023187	Cell division cycle 27 homolog
Mad1l1	1.428	NM_010752	Mitotic arrest deficient 1-like 1
Trip13	1.424	AK010336	Thyroid hormone receptor interactor 13
Depdc1b	1.401	AK077676	DEP domain containing 1B
Growth			
Skp2	1.557	NM_013787	S-phase kinase-associated protein 2 (p45)
Pdgfd	1.555	AK003359	Platelet-derived growth factor, D polypeptide
Ash1l	1.508	AK031724	Ash1 (absent, small, or homeotic)-like
Tgfbi	1.505	NM_009369	Transforming growth factor, beta induced
Il15ra	1.422	NM_008358	Interleukin 15 receptor, alpha chain
Sema4g	1.36	NM_011976	Semaphoring 4G
Fndc1	1.323	AK003938	Fibronectin type III domain containing 1
Gdf15	1.322	NM_011819	Growth differentiation factor 15
Immunity and defense			
Zbtb7a	2.519	NM_010731	Zinc finger and BTB domain containing 7a
Chd3	2.276	AK045449	Chromo domain helicase DNA binding protein 3
Klf3	2.202	NM_008453	Kruppel-like factor 3 (basic) (Klf3), mRNA.
Ifi205	1.597	NM_172648	Interferon activated gene 205
Arrdc4	1.588	AK010022	Expressed sequence AV216361
Blnk	1.552	Y17159	B-cell linker
Soat1	1.46	BC025091	Sterol O-acyltransferase 1
Mst1r	1.439	NM_009074	Macrophage stimulating 1 receptor
Protein kinase activity			
Ptprb	1.842	AF157628	Protein tyrosine phosphatase, receptor type, B
Ttk	1.621	NM_009445	Ttk protein kinase (Ttk), mRNA.
Csnk1a1	1.593	NM_146087	Casein kinase 1, alpha 1
D3Bwg0562e expressed	1.512	AK046782	DNA segment, Chr 3, Brigham & Women's Genetics 0562
Dgkq	1.468	AK077288	Diacylglycerol kinase, theta
Tpk1	1.459	NM_013861	Thiamin pyro phosphokinase
Mst1r	1.439	NM_009074	Macrophage stimulating 1 receptor (c-met-related tyrosine kinase)
Plk4	1.437	L29479	Polo-like kinase 4 (Drosophila)
Prkg2	1.426	NM_008926	Protein kinase, cGMP-dependent, type II
Ppp3cb	1.418	BB372960	Protein phosphatase 3, catalytic subunit, beta isoform
Nucleotide binding			
Gbf1	1.532	BU701920	Golgi-specific brefeldin A-resistance factor 1
Rapgef6	1.432	BC025553	Hypothetical protein A530068K01
Cdc42ep3	1.382	NM_026514	CDC42 effector protein (Rho GTPase binding) 3
Abcc2	1.378	NM_013806	ATP-binding cassette, sub-family C (CFTR/MRP), member 2

Table 2. List of inhibited genes of MC3T3 cells by FIR energy

Gene name	Fold change	Acc.No	Description
Transcription			
Lass6	-3.257	AK028849	Longevity assurance homolog 6
Stat4	-1.742	NM_011487	Signal transducer and activator of transcription 4
Ehox	-1.675	NM_021300	ES cell derived home box containing gene
Usf2	-1.644	NM_011680	Upstream transcription factor 2
Tcf23	-1.595	NM_053085	Transcription factor 23
Nkx6-2	-1.567	AK008173	Inositol polyphosphate-5-phosphatase A
Myt1l	-1.524	NM_008666	Myelin transcription factor 1-like
Prrx1	-1.508	AK038524	Paired related home box 1
Tlx2	-1.418	NM_009392	T-cell leukemia, home box 2
Spic	-1.412	NM_011461	Spi-C transcription factor
Cell –cell signaling			
Pdgfb	-2.304	NM_011057	Platelet derived growth factor, B polypeptide
Il17b	-1.631	NM_019508	Interleukin 17B
Gpbar1	-1.567	NM_174985	G protein-coupled bile acid receptor 1
Rgs9	-1.527	NM_011268	Regulator of G-protein signaling 9
Adcy4	-1.524	NM_080435	Adenylate cyclase 4
Il17rc	-1.481	NM_134159	Interleukin 17 receptor C
Il3	-1.471	NM_010556	Interleukin 3
Thrap3	-1.443	AK046010	Thyroid hormone receptor associated protein 3
P2ry12	-1.408	BC027381	Purinergic receptor P2Y, G-protein coupled 12
Growth			
Akt3	-2.421	NM_011785	Thymoma viral proto-oncogene 3
NM_031879	-2.049	NM_031879	Neuronal differentiation related protein (Ndrp), mRNA
Pdgfb	-2.305	NM_011057	Platelet derived growth factor, B polypeptide
Tnfrsf5	-1.880	NM_011611	Tumor necrosis factor receptor superfamily, member 5
Nmyc1	-1.845	NM_008709	Neuroblastoma myc-related oncogene 1
C1qtnf2	-1.656	BC030324	C1q and tumor necrosis factor related protein 2
Egr3	-1.565	NM_018781	Early growth response 3
Tnfrsf18	-1.506	NM_009400	Tumor necrosis factor receptor superfamily, member 18
Sdbcag84	-1.484	NM_025516	Serologically defined breast cancer antigen 84
Rab3a	-1.484	NM_009001	RAB3A, member RAS oncogene family
Myd116	-1.484	NM_008654	Myeloid differentiation primary response gene 116
Arid5b	-1.437	NM_023598	AT rich interactive domain 5B (Mrf1 like)
Rerg	-1.433	BC026463	RAS-like, estrogen-regulated, growth-inhibitor
Immunity and defense			
Tnfrsf5	-1.880	NM_011611	Tumor necrosis factor receptor superfamily, member 5
Gpbar1	-1.567	NM_174985	G protein-coupled bile acid receptor 1
Il3	-1.471	NM_010556	Interleukin 3
Protein kinase activity			
Aatk	-2.049	NM_007377	Apoptosis-associated tyrosine kinase
Mapk8ip1	-1.766	NM_011162	Mitogen activated protein kinase 8 interacting protein 1
Gucy2g	-1.712	AK049940	Guanylate cyclase 2g
Tyk2	-1.629	NM_018793	Tyrosine kinase 2
Mvk	-1.616	NM_023556	Mevalonate kinase
Pak2	-1.565	AI836325	P21 (CDKN1A)-activated kinase 2
Nagk	-1.502	NM_019542	N-acetyl glucosamine kinase
Hk1	-1.488	NM_010438	Hexokinase 1
Pip5k2c	-1.456	NM_054097	Phosphatidylinositol-4-phosphate 5-kinase, type II, gamma
Limk2	-1.445	NM_010718	LIM motif-containing protein kinase 2
Mark2	-1.445	NM_007928	MAP/microtubule affinity-regulating kinase 2
Ilk	-1.435	NM_010562	Integrin linked kinase
Cdk4	-1.422	AK003804	Cyclin-dependent kinase 4
Nucleotide binding			
Arhgef19	-1.541	AK053075	Rho guanine nucleotide exchange factor (GEF) 19
Abcf1	-1.504	AF213383	ATP-binding cassette, sub-family F (GCN20), member 1
Arhgef1	-1.486	NM_008488	Rho guanine nucleotide exchange factor (GEF) 1
Gna13	-1.471	NM_010303	Guanine nucleotide binding protein, alpha 13

their recent study, Hawkins et al focused into the benefits of using an FIR emitting light combination with laser therapy[33]. Then, it was clarified that fibroblast cell proliferation was increased with expression of FGF and ALP enzyme activity by the effect of FIR on water molecule. Therefore, osteoblast differentiation and bone nodules might be activated by this mechanism.

It was suggested that FIR radiation also activated the Runx2, Osterix, BSP, Col1a1, OCN and OPN genes expression levels through osteoblast differentiation in the present study. The runt family transcription factor of Cbfa1 plays a crucial role and regulates the new bone formation during the early embryogenesis[34]. It have been reported that gene expression and cellular protein levels of Runx2, Osterix, and TGF beta Increased in early embryos of human and murine osteoblast[35, 36]. Therefore, in our results showed that Runx2, Osterix and BSP of FIR treatment group had remarkable higher level expression on early stage[37]. OCN levels were greatly elevated in early stage. Also, Runx2, Col1a1 and OPN revealed significant increased at the end stages of culture. It was suggested that FIR quickly increase the levels of osteogenic specific genes to activate directly bone differentiation.

It was made clear that the gene expression of microarray data showed Smad 7, Tgfbi, VEGF related Chd3, Sp100, DEAD related Ddx 46, 58, Thyroid hormone related Trip13, PDGE related Pdgfd Interleukin related IL15ra, Fndc1 and Sema 4a, Sema 4g were clearly activated. It was reported that *Smad 7* bound the BMP1 receptor to inhibit differentiation of osteoblast by Smad pathway[38,39]. Therefore, it was suggested that Sp100 and Chd3 activated the gene expressions of Runx2 and Osterix to precede the differentiation of osteoblast by Notch pathway.

The differences in the chromatographic or electrophoretic properties of ALP in serum and another tissue have been reported. It was suggested that ALP enzymes transport inorganic phosphatase at the membrane cells matrix vesicle[40]. Moretti G and Mescon H reported the presence of acid phosphatase in the human skin by *Gomori's Technic* and supposed to indicate that sites of AP activity are light brown to black[41]. Rabinovitch M and Andreucci D described the reaction of AP and ALP localized in nuclear in normal human bone marrow cells[42]. In the present study, we found that ALP and AP showed different localization. In addition, though AP was activated initial stage of osteoblast differentiation, ALP activity was late. It was well known that the osteoblast differentiated the osteocyte to absorb the peripheral bone minerals for control the blood calcium ions. The osteocyte had high activity of both ALP and AP. It was clarified that early stage of osteoblast have high activity of both ALP and AP to be activate by FIR radiation in the present study. These finding suggested that AP was important even in osteoblast to absorb minerals and early differentiation of mature osteoblasts.

It was suggested that natural FIR ceramics and compound of titanium and natural FIR ceramics activated new bone formation and vascularization. The FIR ceramics was the excellent radiator which radiation rate was almost 90 % of FIR energy of 5~20 μm and good scaffold for cell migration. There are several reports that FIR radiation has beneficial effects for the treatment, repair and restoration of angiogenesis related diseases. Yu SY et al suggested that the beneficial effect of FIR therapy activated the skin blood flow and AVF patency by the L-arginine/ nitric oxide pathway[43]. The FIR whole body radiation affected the skin microcirculation to improve sleep state and accelerate growth factors[44]. The mechanism of bioactivity for any materials is dependent on content of compounds, surface of chemistry, capacity of ionic dissolution and topology. Natural FIR ceramics radiating FIR energy are the powerful antioxidant to bind to bone due to the rapid formation of a hydroxyapatite the surface layer upon contact with body fluid and are thought to stimulate osteogenesis via their dissolution products[28,37].

Still more, both of soluble silicate and calcium ions are proposed to stimulate osteoprogenitor cells at the implant site[45]. It was also reported that bioactive glasses contains including more than 60-70% silicate dioxide (SiO_2)[46]. But, bioactive glasses ceramics mechanism was staid unclear. Midha S et al reported the benefits of 70S30C bioactive glass scaffolds were highly supported due to calcium ion dissolution and insufficient fluid transport to dampen the pH rise[47]. Therefore, we considered that main role of rhyolite ceramics contains of SiO_2 is bound to injured bone between implanted sites to induce bone formation. In our present study, high dose composite compound and additionally FIR treatment groups were strongly activated cell migration, new vascularization and promoted new bone formation.

In conclusion, FIR precedes the cell differentiation of osteoblast and bone nodules formation with AP and ALP. Maintaining of bone mass and normal remodeling was supported by the effect of FIR with osteogenic gene.

Acknowledgements

I would like to express my appreciation to Professor Seiichiro Kitamura and my supervisor Dr. Kikuji Yamashita and all members of our laboratory. We give our gratitude to Mr. Hirofumi Niki, Mr. Hideaki Horikawa and Ms Hiroko Hagita for the kind support on my experimental technique and research work.

References

1. Neve A, Corrado A and Cantatore FP. Osteoblast physiology in normal and pathological conditions. J Cell Tissue 2: 289-302, 2011
2. Stains JP and Civitelli R. Gap junctions in skeletal development and function. Biochim Biophys Acta 1719: 69-81, 2005
3. Kusumbe AP, Ramasamy SK and Adams RH. Coupling of angiogenesis and osteogenesis by a specific vessel subtype

in bone. Nature 13145: 323-328, 2014
4. Karsenty G and Ferron M. The contribution of bone to whole-organism physiology. Nature 10763: 314-320, 2012
5. Li B and Aspden RM. Composition and mechanical properties of cancellous bone from the femoral head of patients with osteoporosis or osteoarthritis. J Bone Miner Res 12: 641-51, 1997
6. Hollier LH, Sharabi SE, Koshy JC and Stal S. Facial trauma: general principles of management. J Craniofac Surg 21: 1051-1053, 2010
7. Ohtsuki C, Kamitakahara M and Miyazaki T. Bioactive ceramic-based materials with designed reactivity for bone tissue regeneration. J R Soc Interface 6: 349-360, 2009
8. Dimitrievska S, Petit A, Ajji A, Bureau MN and Yahita LH. Biocompatibility of novel polymer-apatite nanocomosite fibers. J Biomed Mater Res 84: 44-53, 2008
9. Tazi N, Zhang Z, Messaddeq Y, Lopes LA, Zanardi LM, Levinson D and Rouabhia M. Hydroxyapatite bioactivated bacterial cellulose promotes osteoblast growth and the formation of bone nodules. AMB Express 2: 61-71, 2012
10. Gao Sh, Shiota M, Fuji M, Chen K, Shimogishi M, Sato M and Kasugai Sh. Combination of simvastatin and hydroxyapatite fiber induce bone augmentation. J Reg Med 2: 53-60, 2013
11. Campion CR, Chander C, Buckland T and Hing K. Increasing strut porosity in silicate substituted calcium-phosphate bone graft substitutes enhances osteogenesis. J Biomed Mater Res Part B: Appl Biomater 97B: 245–254, 2011
12. Shubayev VI, Branemark R, Steinauer J and Myers RR. Titanium implants induce expression of matrix metalloproteinases in bone during osseointegration. J Reh Res Dev 41: 757-766, 2004
13. Yamaguchi M, Inamoto K and Suketa Y. Effect of essential trace metals on bone metabolism in weanling rats: Comparison with zinc and other metals actions. Res Exp Med 186: 337-342, 1986
14. Merolli A, Leali PT, Guidi PL and Gabbi C. Comparisons in *in vivo* response between a bioactive glass and a non-bioactive glass. J Mate Sci Mater Med 11: 219-222, 2000
15. Vogel M, Voigt C, Gross UM and Christian MMM. *In vivo* comparison of bioactive glass particles in rabbits. Biomaterials 22: 357-362, 2001
16. Rahaman MN, Day DE and Tomsia AP. Bioactive glass in tissue engineering. Acta Biomater 7: 2355-2373, 2011
17. Oonishi H, Hench LL, Wilson J, Sugihara F, Tsuji E, Matsuura M, Kin S, Yamamoto T and Mizokawa S. Quantitative comparison of bone growth behavior in granules of bioglass, A-W ceramic, and hydroxyapatite. J Biomed Mater Res 51: 37-46, 2000
18. Chen QZ, Thompson ID and Boccaccini AR. 45S5 bioglass-derived glass-ceramic scaffolds for bone tissue engineering. Biomaterials 27: 2414-2425, 2006
19. Bitto A, Minutoli L, Galeano MR, Altavilla D, Polita F, Fiumara T, Calo M, Cascio PL, Zentilin L, Giacca M and Squadrito F. Angiopoietin-1 gene transfer improves impaired wound healing in genetically diabetic mice without increasing VEGF expression. Clin Sci 114: 707-718, 2008
20. Bocchi L, Evangelisti A, Barrella M, Scatizzi L and Bevilacqua M. Recovery of 0.1 HZ microvascular skin blood flow in dysautonomic diabetic (type 2) neuropathy by using frequency rhythmic electrical modulation system (FREMS). Med Eng Phys 32: 407-413, 2010
21. Hosokawa H, Yamashita K, Ishibashi J, Ishikawa N, Morimoto H, Ishikawa T, Kitamura S and Nagayama M. Anew animal raiser: Effect of low temperature narrow wavelength far infrared radiation on tumor growth of A431 cells. ITE Lett 6: 597-602, 2005
22. Yang CS, Yeh CH, Tung CL, Chen MY, Jiang CH and Yeh ML. Impact of far-infrared ray exposure on the mechanical properties of unwounded skin of rats. Exp Biol Med 235: 952-956, 2010
23. Yamashita K. The effects of the far-Infrared ray (FIR) energy radiation on living body. In: Blood cell an overview of Eng studies in hematology, ed by Moschandreou TE, InTech., Croatia, 2012, pp 271-302.
24. Yamashita K, Hosokawa H, Ishibashi J, Ishikawa N, Morimoto H, Ishikawa T, Nagayama M and Kitamura S. Development of CO_2 incubator with limited far-infrared radiation for activation of mitochondrial metabolism. ITE Letters 6: 468-472, 2005
25. Ishikawa T, Ishibashi J, Yamashita K, Dalkhsuren Sh, Sumida K, Masui T and Kitamura S. Non-thermal effects of far-infrared ray (FIR) on human hepatocellular carcinoma cells HepG2 and their tumors. J Cancer Sci Ther 1: 78-82, 2009
26. Lee JH, Roh MR and Lee KH. Effects of infrared radiation on skin photo-aging and pigmentation. Yonsei Med J 47: 485-490, 2006
27. Udagawa Y and Nagasawa H. Effects of far-infrared ray on reproduction, growth, behavior and some physiological parameters in mice. In vivo 14: 321-326, 2000
28. Inoue S and Kabaya M. Biological activities caused by far-infrared radiation. Int JBiometeorol 33: 145-150, 1989
29. Leung TK, Lee CM, Wu CH, Chiou JF, Huang PJ, Shen LK, Hung CS, Ho YS, Wang HJ, Kung CH, Lin YH and Yeh HM . Protective effects of non-ionized radiation from far infrared ray emitting ceramic material (cFIR) against oxidative stress on human breast epithelial cells. J Med Biol Eng 34: 69-75, 2012
30. Huang PH, Chen JW, Lin CP, Chen YH, Wang CH, Leu HB and Lin SJ. Far infra-red therapy promotes ischemia-induced

angiogenesis in diabetic mice and restores high glucose-suppressed endothelial progenitor cell functions. Cardiovasc Diabetol 11: 99-112, 2012

31. Inoue S, Takemoto M, Chishaki A, Ide T, Nishizaka M, Miyazono M, Sawatari H and Sunagawa K. Leg heating using infra-red radiation in patients with chronic heart failure acutely improves the hemodynamics, vascular endothelial function and oxidative stress. Intern Med 51: 2263-2270, 2012
32. Sheppard AR, Swicord ML and Balzano Q. Quantitative evaluations of mechanisms of radiofrequency interactions with biological molecules and processes. Health Phys 95: 365-396, 2008
33. Hawkins D and Abrahamse H. Influence of broad-spectrum and infrared light in combination with laser irradiation on the proliferation of wounded skin fibroblasts. Photomed Laser Surg 25: 159-169, 2007
34. Ducy P, Zhang R, Geoffroy V, Ridall AL and Karsenty G. Osf2/Cbfa1: A transcriptional activator of osteoblast differentiation. Cell 89: 747-754, 1997
35. Bayers BA and Garcia AJ. Exogenous Runx2 expression enhances in vitro osteoblastic differentiation and mineralization in primary bone marrow stromal cells. Tissue 10: 1623-1632, 2004
36. Zhu F, Friedman MS, Luo W, Woolf P, and Hankenson KD. The transcription factor Osterix (Sp7) regulates BMP6-induced human osteoblast differentiation. J Cell Physiol 227: 2677-2685, 2012
37. Tsai MT, Lin YS, Chen WC, Ho CH, Huang HL and Hsu JT. Runx2 and Osterix gene expression in human bone marrow stromal cells are mediated by far-infrared radiation. World Cong Eng 3: 2690-2694, 2011
38. Al-Aql ZS. Alaql AS, Graves DT, Gerstenfeld LC and Einhorn TA. Molecular mechanisms controlling bone formation during fracture healing and distraction osteogenesis, J Dent Res 87: 107-118, 2008
39. Tang SY and Alliston T. Regulation of postnatal bone homeostasis by TGFβ. BoneKEy reports 2013: doi:10.1038/2012/255
40. Golub EE and Battaglia KB. The role of alkaline phosphatase in mineralization. Curr Opin Orthop 18: 444-448, 2007
41. Moretti G and Mescon H. Histochemical distribution of acid phosphatases in normal human skin. J Invest Derma 26: 347-360, 1956
42. Rabinovitch M and Andreucci D. A histochemical study of Acid and Alkaline phosphatase distribution in normal human bone marrow smears. Blood 4: 580-594, 1949
43. Yu SY, Chiu JH, Yang SD, Hsu YC, Lui WY and Wu CW. Biological effects of far-infrared therapy on increasing skin microcirculation in rats. Photodermatol Photoimmunol Photomed 22: 78-86, 2006
44. Honda K and Inoue S. Sleep-enhancing effects of far-infrared radiation in rats. Int J Biometeorol 32: 92-94, 1988
45. Hardenbrook MA and Lombardo SR. Silicate-substituted calcium phosphate as a bone void filler after kyphoplasty in a young patient with multiple compression fracture due to osteogenesis imperfect variant. Neurosurg Foc 21(6): 1-5, 2006
46. Hench LL. The story of bioglass. J Mater Sci: Mater Med 17: 967-978, 2006
47. Midha S, Kim TB, Bergh WVD, Lee PD, Jones JR and Mitchell CA. Preconditioned 70S30C bioactive glass foams promote osteogenesis in vivo. Acta Biomater 9: 9169-9182, 2013